Chinese Chemical Letters 37 (2026) 111889

Contents lists available at ScienceDirect

Chinese Chemical Letters

journal homepage: www.elsevier.com/locate/cclet

Water-soluble thiazolo[5,4-*d*]thiazole-based AIEgens for universal and Level 3 resolved latent fingerprint visualization

Yumei Wu[a], Zhengjun Chen[a], Yuan Shen[a], Deying Tang[a], Huaiyu Mo[a], Zihan Chen[a], Hongyu Li[a], Zhe Zheng[b,*], Chunju Li[b,c], Jie Gao[a,*], Zeli Yuan[a,*]

[a] *School of Pharmacy, Key Laboratory of Basic Pharmacology of Ministry of Education and Joint International Research Laboratory of Ethnomedicine of Ministry of Education, Guizhou International Science & Technology Cooperation Base of Medical Optical Theranostics Research, Zunyi Medical University, Zunyi 563003, China*

[b] *College of Chemistry, Tianjin Key Laboratory of Structure and Performance for Functional Molecules, Tianjin Normal University, Tianjin 300387, China*

[c] *Academy of Interdisciplinary Studies on Intelligent Molecules, Tianjin Normal University, Tianjin 300387, China*

ARTICLE INFO

Article history:
Received 12 June 2025
Revised 22 September 2025
Accepted 23 September 2025
Available online 24 September 2025

Keywords:
Latent fingerprints
Aggregation-induced emission
Thiazolo[5,4-*d*]thiazole
Level 3 visualization
Fluorescence

ABSTRACT

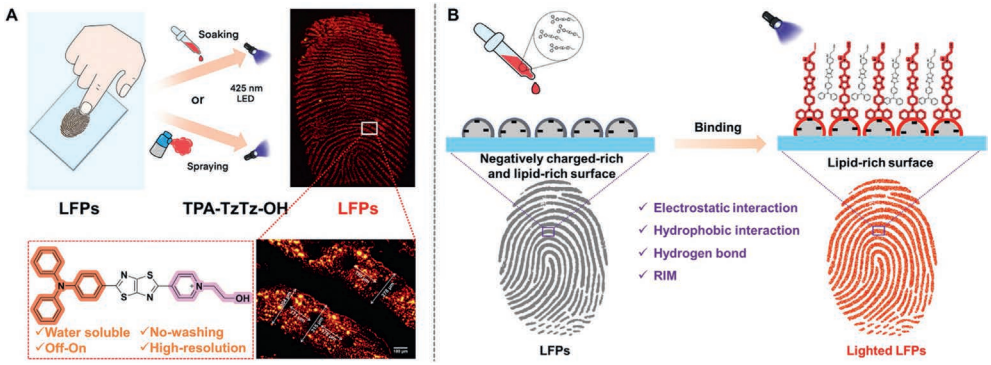
Latent fingerprints (LFPs) serve as indispensable forensic evidence, yet achieving visualization to Level 3 detail, crucial for conclusive identification, remains highly challenging due to poor contrast, substrate limitations, operational toxicity, and aggregation-caused quenching of classic methods. Here, we present a water-soluble thiazolo[5,4-*d*]thiazole (TzTz)-based aggregation-induced emission (AIE) luminogen, TPA-TzTz-OH, rationally designed to address these issues. This probe, integrating triphenylamine electron donors, a TzTz π-bridge, and a pyridinium acceptor, enables a distinctive fluorescence "off−on" switch upon visible light (425 nm) excitation, visualizing LFPs within 40 s, completely avoiding organic solvents or post-processing. TPA-TzTz-OH offers broad substrate compatibility, producing high-contrast, high-fidelity fingerprint images on metals, glass, plastics, ceramics, and wood, consistently resolving sweat pores and ridge microstructures (Level 3 features) essential for individualization. Mechanistic studies indicate that restricted intramolecular motion upon specific binding to fingerprint lipids (oleic acid and cholesterol) triggers pronounced AIE enhancement, with electrostatic and hydrogen-bonding interactions enabling specificity. The probe exhibits excellent biocompatibility (>85% cell viability at working concentration), retains efficacy for aged fingerprints (≥10 days), and can be used *via* immersion or spraying. Comparison with control derivatives confirms the synergistic importance of both the pyridinium charge and hydroxyl group in realizing these unique advantages. This work establishes TPA-TzTz-OH as a promising, sustainable solution for high-resolution forensic visualization, bridging fundamental AIE photophysics and real-world criminalistics while providing a greener and safer technique over conventional methods.

© 2026 Published by Elsevier B.V. on behalf of Chinese Chemical Society and Institute of Materia Medica, Chinese Academy of Medical Sciences.

Fingerprints are fundamental to forensic identification due to their uniqueness and lifetime stability [1]. However, latent fingerprints (LFPs), the invisible residues left upon contact, present persistent challenges for reliable visualization due to their fragility, potential degradation, and the diversity of substrates encountered [2–5]. Conventional approaches, including powder dusting, chemical fuming, mass spectrometry, and various spectroscopic techniques [6–9], often suffer from drawbacks such as complex protocols, risk of evidence damage, high cost, or significant background interference. In this context, fluorescence-based methods have emerged as a powerful alternative, offering high sensitivity and spatial resolution (Table S1 in Supporting information) [4,10–15]. A variety of fluorescent materials, including quantum dots, upconversion nanoparticles, and metal-organic frameworks, have advanced LFP detection [3,6,16–19]. Among these, luminogens exhibiting aggregation-induced emission (AIE), termed AIEgens, are particularly attractive due to their strong emission in the aggregated state and high chemical tunability [20–27]. Despite progress, many existing systems are still limited by powder-induced ridge damage [28], reliance on organic co-solvents, "always-on" background fluorescence requiring wash steps, and the need for potentially damaging ultraviolet (UV) excitation. Crucially, resolving Level 3 details, such as sweat pores and ridge edge features, remains a significant hurdle. Therefore, a robust, water-soluble probe that enables visible-light-excited, "off–on" fluorescence for rapid, high-contrast imaging of Level 3 features in a pure aqueous system is highly desirable.

* Corresponding authors.
E-mail addresses: zhezheng@tjnu.edu.cn (Z. Zheng), jiegao@zmu.edu.cn (J. Gao), zlyuan@zmu.edu.cn (Z. Yuan).

https://doi.org/10.1016/j.cclet.2025.111889
1001-8417/© 2026 Published by Elsevier B.V. on behalf of Chinese Chemical Society and Institute of Materia Medica, Chinese Academy of Medical Sciences.



Scheme 1. Schematic representation of (A) the experimental setup and (B) the proposed mechanism for LFPs visual imaging using the TPA-TzTz-OH probe applied *via* soaking or spraying.

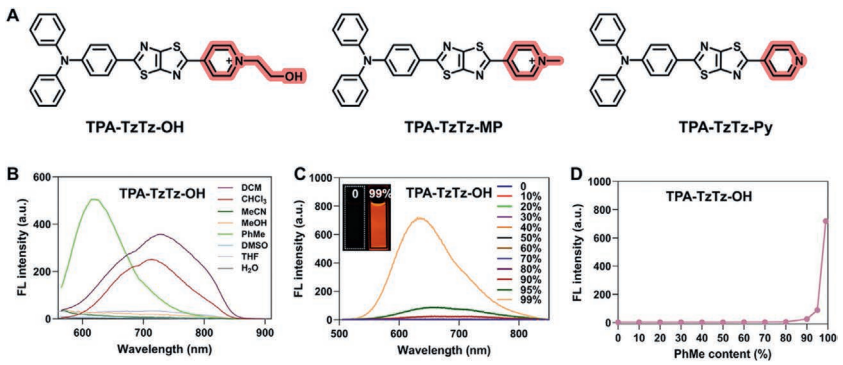


Fig. 1. (A) Molecular structures of TPA-TzTz-Py, TPA-TzTz-MP, and TPA-TzTz-OH. (B) Fluorescence spectra of TPA-TzTz-OH (10 μmol/L) in different solvents. (C) Fluorescence emission spectra of TPA-TzTz-OH (10 μmol/L) in PhMe/DMSO mixtures with varying volume fractions of PhMe (f_{PhMe}, 0–99 %). Inset: Fluorescent photographs of TPA-TzTz-OH under illumination (λ_{ex} = 425 nm) in pure DMSO (f_{PhMe} = 0 %, left) and a PhMe/DMSO mixture (f_{PhMe} = 99 %, right). (D) Fluorescence variation of TPA-TzTz-OH in PhMe/DMSO mixture 0 %–99 % f_{PhMe}.

Here, we leveraged thiazolo[5,4-*d*]thiazole (TzTz), a rigid, electron-deficient heterocycle known to facilitate restriction of intramolecular motion (RIM) and provide multiple noncovalent interaction sites [29–33]. By embedding TzTz into a donor–π–acceptor (D–π–A) framework, we anticipated strengthening the intramolecular charge transfer (ICT) effect, further restricting molecular motion upon binding, and promoting specific interactions with LFP components. We now report TPA-TzTz-OH, a probe integrating a triphenylamine (TPA) donor, a TzTz π-bridge, and a pyridinium acceptor (Scheme 1). This design provides visible-light (425 nm) excited "off–on" fluorescence, enables rapid LFP development in pure water, and achieves reliable Level 3 visualization across various substrates. Mechanistic investigations indicate that its fluorescence is activated by binding-triggered RIM in the presence of fingerprint lipids, yielding exceptional contrast and photostability.

Our design targeted a water-soluble AIE probe with selective affinity for LFP residues and a robust turn-on mechanism under visible light. The TzTz bridge was chosen for its propensity to support RIM and noncovalent interactions, while the TPA group supplies the AIE characteristic, and the pyridinium salt imparts water solubility and electrostatic attraction. A terminal hydroxyl group was introduced to enhance hydrogen bonding with fatty acids and amino acids in fingerprints. To deconvolute the contributions of charge and the hydroxyl group, two control molecules, TPA-TzTz-Py (neutral) and TPA-TzTz-MP (cationic, no –OH), were also prepared (Fig. 1A). TPA-TzTz-Py was synthesized *via* a one-pot condensation reaction (Scheme S1 in Supporting information, 16.7 % yield). Subsequent *N*-alkylation with 2-bromoethanol or iodomethane afforded TPA-TzTz-OH (99.6 % yield) and TPA-TzTz-MP (69.5 % yield), respectively. All structures were rigorously confirmed by nuclear magnetic resonance spectroscopy and high-resolution mass spectrometry (Figs. S1–S9 in Supporting information). Detailed synthetic procedures and characterization data are provided in the Supporting information.

TPA-TzTz-OH demonstrated high water solubility (up to 200 μmol/L) and good photostability (Fig. S10 in Supporting information). In good solvents such as water or DMSO, the probe was weakly emissive (Fig. 1B). To induce aggregation, solvent polarity was tuned using PhMe/DMSO mixtures; in a mixture with a PhMe fraction (f_{PhMe}) of 99 %, the fluorescence at 631 nm increased approximately 65-fold, confirming its AIE nature (Figs. 1C and D). The photoluminescence quantum yield rose from 0.19 % in pure DMSO to 12.43 % in the aggregated state (f_{PhMe} = 99 %) (Table S2 in Supporting information). Spectroscopic analysis revealed a maximum absorption at 480 nm in DMSO (Table S2 in Supporting information), while the solid-state photoluminescence peaked at 784 nm, indicating potential near-infrared emission capabilities (Fig. S11 and Table S2 in Supporting information). The control probe TPA-TzTz-MP exhibited analogous AIE behavior (Fig. S12 in Supporting information). Density functional theory calculations (Fig. S13 in Supporting information) revealed that *N*-alkylation lowers the highest occupied molecular orbital (HOMO) – lowest unoccupied molecular orbital (LUMO) energy gaps for TPA-TzTz-OH and TPA-TzTz-MP (E_g = 1.60 eV) relative to the neutral TPA-TzTz-Py (E_g = 2.94 eV), in agreement with the observed spectral shifts. Electrostatic potential (ESP) maps confirmed the localized positive charge on the quaternized probes.

To evaluate its primary application, fresh LFPs on glass slides were treated with 100 μmol/L aqueous solutions of the probes for 60 s. Under 425 nm excitation, TPA-TzTz-OH rapidly developed

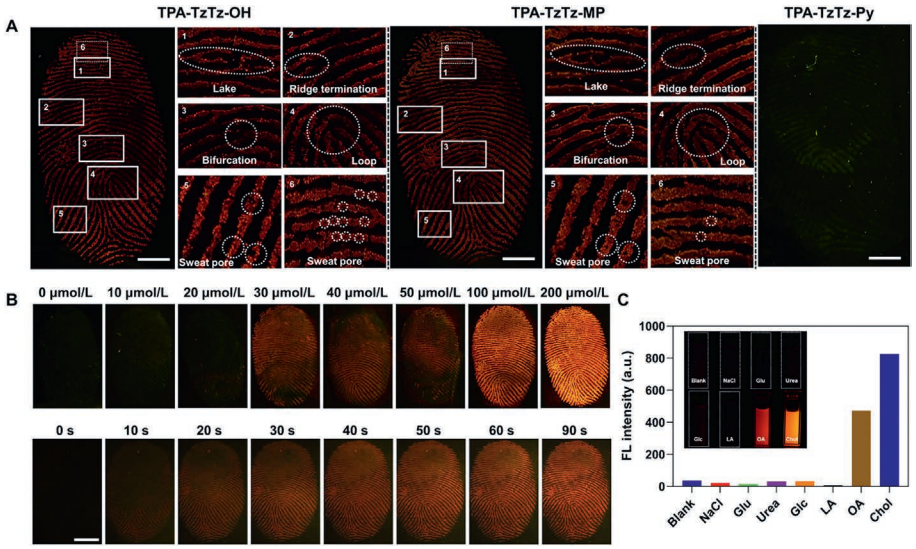


Fig. 2. Visualization of LFPs using AIE-active TzTz probes. (A) High-resolution fluorescence images showcasing Levels 1, 2, and 3 details of LFPs deposited on glass slides, developed using aqueous solutions (100 μmol/L) of TPA-TzTz-OH, TPA-TzTz-MP, and TPA-TzTz-Py (scale bar: 3 mm). (B) Optimization of LFP visualization on glass using TPA-TzTz-OH. Top: Fluorescence images demonstrating the effect of varying probe concentration. Bottom: Fluorescence images illustrating the impact of immersion time using a 100 μmol/L aqueous solution (λ_{ex} = 425 nm; scale bar: 5 mm). (C) Fluorescence intensity of TPA-TzTz-OH (10 μmol/L in DMSO/water, 1:1 v/v) upon addition of various substances commonly found in LFPs. Inset: corresponding photographs under 425 nm irradiation. Corresponding grayscale images are shown in Fig. S25 (Supporting information).

high-definition ridge patterns with clearly resolved Level 3 features (Fig. 2A). In contrast, TPA-TzTz-MP produced red emission but visualized fewer pores, while the neutral TPA-TzTz-Py yielded only faint outlines. The corresponding signal-to-noise ratios (SNRs) were 15.6, 15.3, and 1.3, respectively (Fig. S14 in Supporting information), quantifying the superior performance of TPA-TzTz-OH. Furthermore, the cell counting kit-8 (CCK-8) assays demonstrated that TPA-TzTz-OH maintained over 85 % cell viability at concentrations up to 100 μmol/L, confirming its low cytotoxicity (Fig. S15 in Supporting information). Optimization studies showed that a concentration of 100 μmol/L was optimal for resolving sweat pores (Fig. 2B and Fig. S16 in Supporting information). Time-dependent experiments revealed that development produced visible outlines within 20 s and clear details by ~40 s (Video S1 and Fig. S17 in Supporting information), highlighting the potential for rapid, real-time LFP analysis.

To elucidate the sensing mechanism, we investigated the probe's response to representative LFP components (Fig. 2C, Figs. S18 and S19 in Supporting information). TPA-TzTz-OH exhibited a strong fluorescence turn-on exclusively in the presence of oleic acid (OA) and cholesterol (Chol). The control probe TPA-TzTz-MP also responded to OA and Chol but with a significantly attenuated signal for Chol, underscoring the hydroxyl group's crucial role in Chol recognition. Conversely, the neutral TPA-TzTz-Py responded only to Chol, indicating that the cationic charge is essential for binding OA. These selectivities were visually confirmed by imaging patterns written with each component (Fig. S19). In addition, to demonstrate the electrostatic attraction between TPA-TzTz-OH and fingerprint residues, we measured the zeta potential of TPA-TzTz-OH, obtaining a value of (34.50 ± 4.57) mV. Based on these results, we propose a multi-interaction binding mechanism: (1) Electrostatic attraction between the pyridinium cation and the carboxylate of OA; (2) hydrogen bonding involving the terminal hydroxyl group and TzTz heteroatoms, which is critical for Chol binding; and (3) hydrophobic contacts with the lipid segments. This targeted binding effectively restricts intramolecular motions, which suppresses non-radiative decay pathways, thus activating the AIE fluorescence and producing high-contrast images against a dark background.

Treatment of LFPs with TPA-TzTz-OH provided high-resolution visualization of papillary ridge patterns (Fig. 3). Magnified fluorescence images (Fig. 3A) distinctly resolved features across all three hierarchical levels: Level 1 (overall pattern configuration, *e.g.*, core, delta), Level 2 (minutiae, *e.g.*, ridge endings, bifurcations, lakes, short ridges), and crucially, Level 3 details, encompassing individual sweat pores (poroscopy) and ridge edge contours (edgeoscopy). Analysis of fluorescence intensity profiles across ridge-furrow transitions confirmed the excellent signal-to-background contrast achieved against the substrate. Notably, this comprehensive, multi-level visualization was achieved *via* a simple immersion step using aqueous TPA-TzTz-OH (100 μmol/L, 60 s), requiring no subsequent physical or chemical post-treatments. The ability to consistently resolve Level 3 details is forensically paramount, as fragmentary LFPs frequently encountered at crime scenes often lack sufficient Level 1 or 2 information for definitive identification. In these instances, unique Level 3 characteristics, such as sweat pore configurations (number, position, shape) and ridge edgeology, become indispensable for robust individualization.

To rigorously assess the fidelity of Level 3 feature reproduction, LFPs developed with TPA-TzTz-OH were examined by fluorescence microscopy (Fig. 3B, upper panel). The resulting micrographs provide unambiguous visualization of sweat pore number, precise location, and spatial arrangement along the papillary ridges. Furthermore, subtle variations in inter-pore distances along the same ridge, as well as differences in ridge width, were readily discernible (Fig. 3B, lower panel), highlighting the fine microstructural details captured by the probe. Comparative analysis with scanning electron microscopy (SEM) of similarly prepared LFPs was conducted (Fig. 3C). While SEM reveals surface topography, the fluorescence images generated by TPA-TzTz-OH offered markedly superior contrast specifically for poroscopic features. Sweat pore distribution, clearly delineated in fluorescence micrographs, was considerably more difficult to discern in the corresponding SEM images due to lower intrinsic contrast for these features under the conditions used.

Finally, to validate the anatomical accuracy of the developed LFPs, a direct comparison was made between the fluorescence image of a TPA-TzTz-OH-developed LFP and a bright-field image

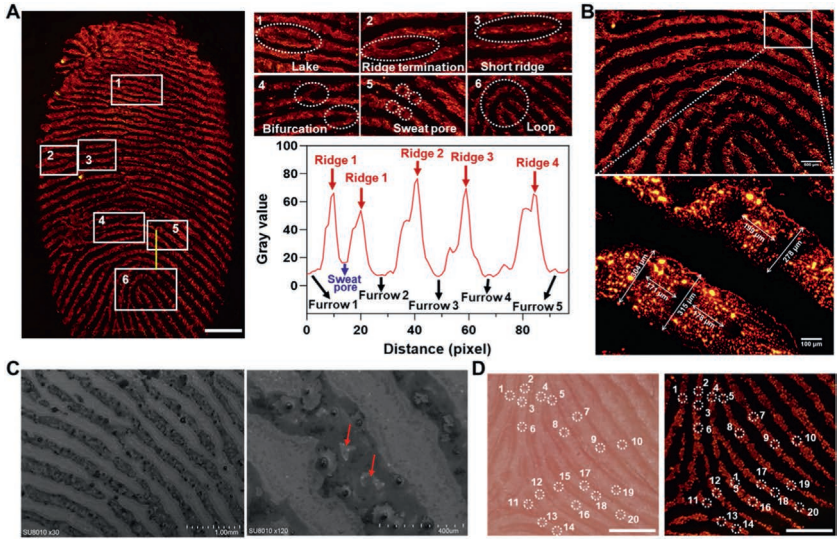


Fig. 3. (A) Levels 1, 2, and 3 details of local LFPs on glass developed by a TPA-TzTz-OH aqueous solution (100 μmol/L) and the variations of the fluorescence intensity between the fingerprint ridges and furrows across the yellow line (scale bar: 2 mm). (B) Fluorescence microscopic images for partial region of the LFPs from a volunteer and the analysis of Level 3 microscopic details. Compared with the images in Fig. 2, the sweat pores and shape of the ridges are visualized with definite sizes. Scale bar: 500 μm (upper), 100 μm (lower). (C) SEM images of the fingerprint on glass, the area indicated by the red arrow is the sweat pore. Scale bar: 1 mm (left), 400 μm (right). (D) Number and location distribution of sweat pores of the real fingerprint (left) on the finger and its developed fingerprint (right) on glass from a volunteer. The fluorescent pattern of the LFPs is much more decipherable than other types (scale bar: 1.5 mm). Corresponding grayscale images are shown in Fig. S26 (Supporting information).

of the corresponding region from the donor's finger (Fig. 3D). This revealed excellent point-by-point correspondence, particularly concerning the number, relative positioning, and arrangement of sweat pores, especially adjacent to minutiae like bifurcations. This high correlation confirms that TPA-TzTz-OH development provides a high-fidelity reproduction of fingerprint microanatomy, enabling reliable individual identification by leveraging crucial Level 3 details. To evaluate the substrate universality of TPA-TzTz-OH for fingerprint imaging, we tested its visualization capabilities on diverse common materials. LFPs were deposited on surfaces including stainless steel (dish base), glass (slide), plastic (sheet), glazed ceramic (bowl base), tinfoil, and wood (comb). Following treatment with aqueous TPA-TzTz-OH (100 μmol/L, 60 s), LFPs were successfully developed on all tested substrates, affording clear fluorescence images with high contrast and resolution (Fig. S20A in Supporting information). Notably, while effective across all materials, the definition of Level 1, 2, and 3 fingerprint details appeared marginally more distinct on smoother, non-porous surfaces such as glass, plastic, ceramic, and foil compared to stainless steel and wood under the experimental conditions. Nevertheless, magnified fluorescence images consistently revealed intricate features across all substrates. Level 1 patterns (*e.g.*, loops), Level 2 minutiae (*e.g.*, lakes, short ridges, bifurcations, ridge endings), and critically, Level 3 details (individual sweat pores) were clearly discernible (Fig. S20B in Supporting information). Quantitative analysis of fluorescence intensity from selected regions further confirmed consistent performance across the different substrates (Fig. S20C in Supporting information). These results collectively demonstrate the robust performance and broad substrate compatibility of TPA-TzTz-OH, highlighting its potential applicability for developing LFPs on a wide range of surfaces encountered in forensic investigations.

The visualization of aged LFPs represents a critical challenge in forensic investigations, as evidence collected from crime scenes frequently includes fingerprints deposited days or weeks prior to discovery. To evaluate the effectiveness of TPA-TzTz-OH in addressing this challenge, we systematically compared its performance in visualizing both fresh and aged (10 days) LFPs deposited on glass surfaces. As demonstrated in Fig. S21 (Supporting information), TPA-TzTz-OH exhibited remarkable consistency in developing both fresh and aged specimens, with no significant degradation in imaging quality observed for the 10-day-old fingerprints. Importantly, fingerprint details across all identification levels, from Level 1 pattern configurations to Level 2 minutiae and the forensically valuable Level 3 features (sweat pores), remained clearly discernible in both cases. This persistence of visualization efficacy underscores the probe's forensic reliability for analyzing fingerprints of varying ages.

The long-term stability of developed fingerprints represents another crucial consideration for evidential documentation and courtroom presentation. Analysis of TPA-TzTz-OH-developed LFPs stored under dark conditions for one month revealed exceptional stability, with negligible changes in both sweat pore detail resolution and overall fluorescence intensity (Fig. S22 in Supporting information). This remarkable preservation of imaging quality facilitates extended examination periods and reliable archiving of processed evidence.

To assess inter-individual robustness, we further evaluated TPA-TzTz-OH's visualization performance on fingerprints collected from multiple donors. Fingerprints obtained from a second volunteer and processed using identical protocols demonstrated consistent high-quality visualization, with Level 3 structural features clearly resolved (Fig. S23 in Supporting information). This donor-independent performance confirms the broad applicability of TPA-TzTz-OH across different fingerprint compositions, which can vary substantially in lipid content and secretion profiles between individuals.

Collectively, these results establish TPA-TzTz-OH as a robust, stable, and versatile AIE probe for LFP visualization, capable of consistently revealing detailed ridge patterns regardless of fingerprint age, storage duration of developed fingerprints, or donor variability, key attributes for practical implementation in forensic casework.

To assess alternative application methodologies with potential for field deployment, we evaluated a spray-based approach for TPA-TzTz-OH application to LFP. LFPs deposited on glass surfaces were treated with an aqueous solution of TPA-TzTz-OH (100 μmol/L) using a hand-held sprayer, with the development process monitored at various time intervals (Fig. S24 in Support-

ing information). The fluorescence intensity of developed fingerprints exhibited a time-dependent enhancement, progressively increasing with extended spray duration. Notably, optimal visualization was achieved at approximately 30 s of application, where Level 1 (pattern configuration), Level 2 (minutiae), and critically, Level 3 (sweat pores) details were clearly resolved with excellent contrast. Interestingly, prolonged spraying (60 s) resulted in diminished resolution of Level 3 features, likely due to excess reagent accumulation causing detail obfuscation. This optimization of the spraying protocol demonstrates the versatility of TPA-TzTz-OH across different application modalities. The successful development of high-resolution fingerprints using both immersion (as described previously) and spray-based techniques highlights the operational flexibility of this AIE probe. The rapid processing time (30 s) and straightforward application methodology of the spray approach offer advantages for on-site fingerprint development at crime scenes, where simplicity and speed are often paramount considerations.

In conclusion, we have developed TPA-TzTz-OH, a water-soluble and eco-friendly AIE probe that enables visible-light-excited, "off–on" visualization of latent fingerprints in pure water. Its selective binding to lipidic residues, namely OA and Chol, triggers a strong fluorescence emission *via* a RIM mechanism, producing high-contrast images with reliable Level 3 resolution in under 40 s. The method is effective across a wide range of common substrates, requires neither organic solvents nor post-processing steps, and exhibits low cytotoxicity at working concentrations. Its demonstrated ability to develop aged fingerprints and yield stable, high-fidelity images makes TPA-TzTz-OH a highly practical and advanced tool for forensic casework.

Ethical statement

This study involved the collection and use of human fingerprint samples. It was conducted in accordance with the ethical principles of the Declaration of Helsinki and was approved by the Medical Ethics Committee of Zunyi Medical University. All participants provided written informed consent after being fully informed of the purpose, procedures, and potential risks of the study. Participant privacy was strictly protected; all personal information was anonymized and used solely for the purposes of this research.

CRediT authorship contribution statement

Yumei Wu: Writing – original draft, Visualization, Validation, Methodology, Investigation, Data curation, Conceptualization. **Zhengjun Chen:** Writing – original draft, Visualization, Validation, Methodology, Investigation, Data curation, Conceptualization. **Yuan Shen:** Writing – original draft, Visualization, Validation, Methodology, Investigation, Data curation, Conceptualization. **Deying Tang:** Investigation, Data curation. **Huaiyu Mo:** Investigation, Data curation. **Zihan Chen:** Investigation, Data curation. **Hongyu Li:** Supervision, Resources, Formal analysis. **Zhe Zheng:** Supervision, Resources, Formal analysis. **Chunju Li:** Writing – review & editing, Methodology, Formal analysis. **Jie Gao:** Writing – review & editing, Methodology, Formal analysis. **Zeli Yuan:** Writing – review & editing, Supervision, Resources, Methodology, Funding acquisition, Conceptualization.

Declaration of competing interest

The authors declare that they have no known competing financial interests or personal relationships that could have appeared to influence the work reported in this paper.

Acknowledgments

This work was supported by the National Natural Science Foundation of China (Nos. 82460614, 62405386, 22301218), Guizhou Provincial Science and Technology Projects (No. QKHJC[2024]Youth321), Science and Technology Innovation Team of Higher Education of Guizhou Provincial Education Department (No. Qianjiaoji [2023]073), Excellent Youth Scientific and Technological Talents of Guizhou Province (No. Qiankehe platform talents [2021]5638), Guizhou Provincial Basic Research Program (Natural Science) (No. Qiankehe Basic MS(2025)353), Zunyi Science and Technology Plan Project (No. Zunshi Keren Platform [2023]2).

Supplementary materials

Supplementary material associated with this article can be found, in the online version, at doi:10.1016/j.cclet.2025.111889.

References

[1] P. Hazarika, D.A. Russell, Angew. Chem. Int. Ed. 51 (2012) 3524–3531.
[2] E.O. Dare, V. Vendrell-Criado, M.C. Jiménez, R. Pérez-Ruiz, D. Díaz Díaz, Chem. Eur. J. 26 (2020) 13142–13146.
[3] R. Chen, F. Fan, L. Peng, et al., Adv. Funct. Mater. 35 (2024) 2418235.
[4] Y. Fang, J.Y. Luan, J.S. Zhao, et al., Chin. J. Chem. 42 (2024) 3337–3342.
[5] E.O. Dare, V. Vendrell-Criado, M.C. Jiménez, R. Pérez-Ruiz, D.Díaz Díaz, Dyes Pigm. 184 (2021) 108841.
[6] M. Wang, M. Li, A. Yu, et al., Adv. Funct. Mater. 27 (2017) 1606243.
[7] L. Xu, Y. Li, S. Wu, X. Liu, B. Su, Angew. Chem. Int. Ed. 51 (2012) 8068–8072.
[8] B. Figueroa, Y. Chen, K. Berry, A. Francis, D. Fu, Anal. Chem. 89 (2017) 4468–4473.
[9] H.W. Tang, W. Lu, C.M. Che, K.M. Ng, Anal. Chem. 82 (2010) 1589–1593.
[10] N. Ruan, Q. Qiu, X. Wei, et al., J. Am. Chem. Soc. 146 (2024) 2072–2079.
[11] Y. Chen, A. Li, X. Li, et al., Adv. Mater. 35 (2023) e2211917.
[12] S. Zhu, H. Liao, T. Guo, et al., Sens. Actuators B: Chem. 433 (2025) 137518.
[13] J. He, Z.H. Pu, X. Dai, et al., Sens. Actuators B: Chem. 418 (2024) 136312.
[14] D. Chen, C. Bao, L. Zhang, et al., Adv. Funct. Mater. 34 (2024) 2314093.
[15] Q. Zhang, F. Cui, X. Dang, et al., Chem. Eur. J. 30 (2024) e202401426.
[16] H. Mardani, S. Mehrbakhsh, S. Sheikhzadegan, M. Babazadeh-Mamaqani, H. Roghani-Mamaqani, ACS Appl. Mater. Interfaces 16 (2024) 1605–1615.
[17] J. Cao, R. Chen, L. Wang, et al., Chem. Eng. J. 491 (2024) 152121.
[18] K. Zhang, M.J. Zhu, Y.W. Zhou, et al., Anal. Chim. Acta 1279 (2023) 341774.
[19] G.R. Mamatha, B.R. Radha Krushna, J. Malleshappa, et al., J. Photochem. Photobiol. A 439 (2023) 114560.
[20] Y.L. Wang, C. Li, H.Q. Qu, et al., J. Am. Chem. Soc. 142 (2020) 7497–7505.
[21] L. Duan, Q. Zheng, T. Tu, Adv. Mater. 34 (2022) e2202540.
[22] P. Zhang, Q. Shen, Y. Zhou, et al., Chin. Chem. Lett. 34 (2023) 107910.
[23] R. Tian, F.Y. Zhu, R. Ma, et al., Biosens. Bioelectron. 263 (2024) 116572.
[24] Z. Jiang, Q. Zhang, Z. Kong, et al., Dyes Pigm. 222 (2024) 111837.
[25] W. Xiao, Q. Zhang, D.H. You, et al., Anal. Chim. Acta 1288 (2024) 342173.
[26] H. Gu, W. Sun, J. Du, J. Fan, X. Peng, Smart Mol. 2 (2023) e20230014.
[27] X. Chen, Y. Jiang, J. Liu, et al., Chem. Biomed. Imaging 2 (2024) 775–783.
[28] Z. Qiu, B. Hao, X. Gu, et al., Sci. China Chem. 61 (2018) 966–970.
[29] N.A. Sayresmith, A. Saminathan, J.K. Sailer, et al., J. Am. Chem. Soc. 141 (2019) 18780–18790.
[30] T.J. Adams, A.R. Brotherton, J.A. Molai, et al., Adv. Funct. Mater. 31 (2021) 2103408.
[31] H. Nie, D. Hu, Z. Zeng, et al., Sci. China Chem. 67 (2024) 1605–1612.
[32] A.R. Brotherton, A. Shibu, J.C. Meadows, et al., Adv. Sci. 10 (2023) e2205729.
[33] A. Thorat, S. Behera, A.A. Boopathi, C. Kulkarni, Angew. Chem. Int. Ed. 63 (2024) e202409725.